

# Nanocurcumin Potently Inhibits SARS-CoV-2 Spike Protein-Induced Cytokine Storm by Deactivation of MAPK/NF- $\kappa$ B Signaling in Epithelial Cells

Vivek K. Sharma,<sup>§</sup> Prateeksha,<sup>§</sup> Shailendra P. Singh, Brahma N. Singh,\* Chandana V. Rao, and Saroj K. Barik\*



Cite This: *ACS Appl. Bio Mater.* 2022, 5, 483–491



Read Online

ACCESS |



Metrics & More



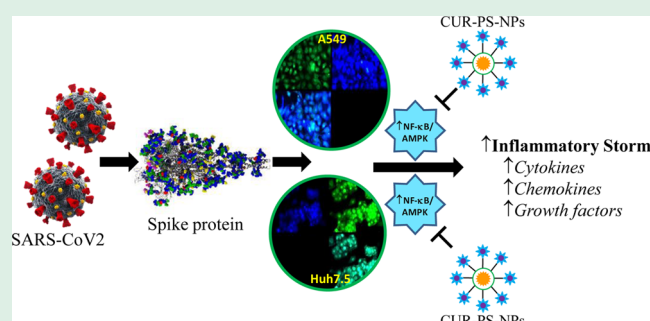
Article Recommendations



Supporting Information

**ABSTRACT:** Interleukin-mediated deep cytokine storm, an aggressive inflammatory response to SARS-CoV-2 virus infection in COVID-19 patients, is correlated directly with lung injury, multi-organ failure, and poor prognosis of severe COVID-19 patients. Curcumin (CUR), a phenolic antioxidant compound obtained from turmeric (*Curcuma longa* L.), is well-known for its strong anti-inflammatory activity. However, its *in vivo* efficacy is constrained due to poor bioavailability. Herein, we report that CUR-encapsulated polysaccharide nanoparticles (CUR-PS-NPs) potently inhibit the release of cytokines, chemokines, and growth factors associated with damage of SARS-CoV-2 spike protein (CoV2-SP)-stimulated liver Huh7.5 and lung A549 epithelial cells. Treatment with CUR-PS-NPs effectively attenuated the interaction of ACE2 and CoV2-SP. The effects of CUR-PS-NPs were linked to reduced NF- $\kappa$ B/MAPK signaling which in turn decreased CoV2-SP-mediated phosphorylation of p38 MAPK, p42/44 MAPK, and p65/NF- $\kappa$ B as well as nuclear p65/NF- $\kappa$ B expression. The findings of the study strongly indicate that organic NPs of CUR can be used to control hyper-inflammatory responses and prevent lung and liver injuries associated with CoV2-SP-mediated cytokine storm.

**KEYWORDS:** nanocurcumin, SARS-CoV-2, spike protein, cytokine storm, MAPK/NF- $\kappa$ B signaling, epithelial cells



## INTRODUCTION

The severe acute respiratory syndrome coronavirus 2 (SARS-CoV-2), the causal organism of coronavirus disease-19 (COVID-19), emerged in December, 2019, and became the most calamitous pandemic of the 21st century.<sup>1</sup> The very high rate of mutation of SARS-CoV-2 continues to pose challenges to the scientific and medical professionals worldwide to effectively control the disease. SARS-CoV-2 relates to the  $\beta$ -coronavirus genus with around 79.5% sequence similarity with the SARS-CoV that appeared in southern China in 2002.<sup>2</sup> The mechanisms so far understood for the COVID-19 progress are characterized by a quick viral replication, resulting in elevated cytolysis of host cells and a hyper-inflammatory state due to excessive production of pro-inflammatory cytokines known as a “cytokine storm” inducing multiple organ damage.<sup>3,4</sup> The cytokine storm is a life-threatening systemic inflammatory syndrome that involves elevated levels of circulating cytokines and immune-cell hyperactivation leading to secondary organ dysfunction, particularly renal, hepatic, or pulmonary. Various pathogens, therapies, cancers, autoimmune conditions, and monogenic disorders have already been reported to trigger such a syndrome in humans.<sup>3</sup>

Angiotensin-converting enzyme 2 (ACE2), a member of dipeptidyl carboxypeptidase group, is widely expressed in different human organs including lungs, kidneys, liver, gut, and vascular systems. It is recognized as a key entry receptor for SARS-CoV-2.<sup>5</sup> The binding of SARS-CoV-2 surface spike protein (CoV2-SP) to human ACE2 through its receptor binding domain triggers a series of physiological events including the cytokine storm through activation of nuclear factor  $\kappa$ B (NF- $\kappa$ B) and mitogen-activated protein kinase (MAPK) by IL-6 trans-signaling.<sup>6,7</sup> This storm induces several pathological complications, particularly acute respiratory distress syndrome (ARDS), often found in serious COVID-19 patients.<sup>8,9</sup> The cytokine storm caused by SARS-CoV-2 is characterized by enhanced levels of IL-6, tumour necrosis factor  $\alpha$  (TNF- $\alpha$ ), and C-C motif chemokine ligand (CCL2).

**Received:** August 6, 2021

**Accepted:** January 16, 2022

**Published:** February 3, 2022



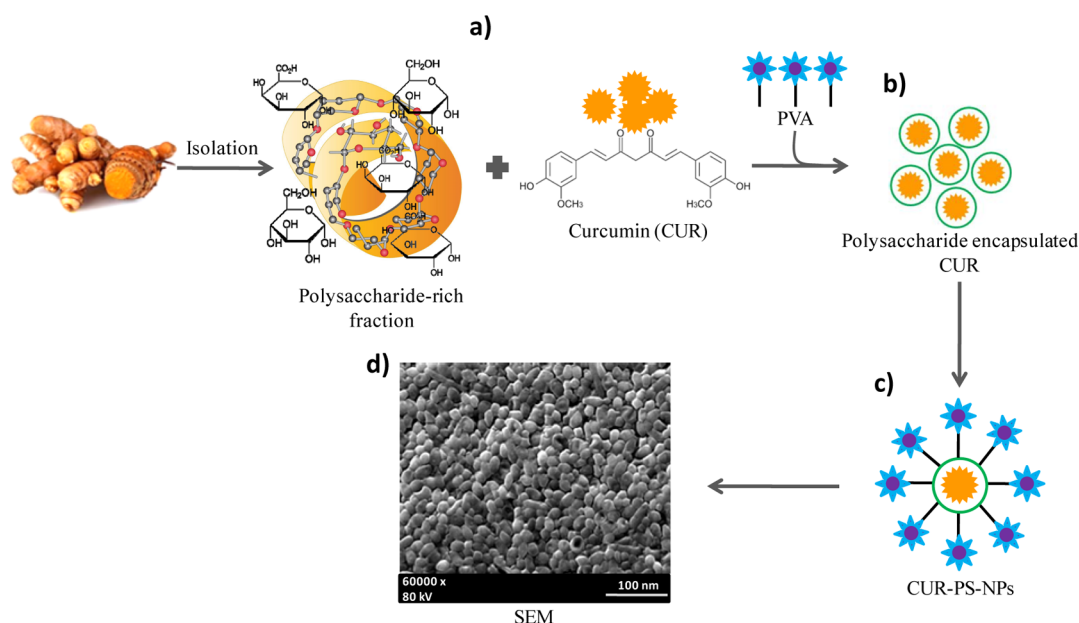


**Figure 1.** CUR–PS-NPs fabrication scheme. (a) Mixing of CUR and polysaccharide-rich fraction isolated from the rhizome of turmeric under stirring conditions at 250 rpm for 120 min. (b) Addition of polyvinyl alcohol solution (1%) to the mixture of CUR and PS. (c) Prepared CUR–PS-NPs. (d) SEM image of CUR–PS-NPs.

The patients with COVID-19-associated ARDS suffer from more organ and tissue injuries, and have greater mortality than the ARDS not related to COVID-19.<sup>8,10</sup> Anti-COVID-19 pharmacological strategy using anti-inflammatory approaches *via* modulating IL-6<sup>11</sup> and IL-8<sup>12</sup> has been quite effective. Therefore, discovery of compounds having the ability to inhibit cytokine storms, and to understand the mechanisms of their anti-inflammation activity can help development of effective anti-COVID-19 drugs.

Curcumin (CUR), a key dietary polyphenolic compound predominantly present in the rhizome of turmeric plant (*Curcuma longa* L.), exhibits a range of biological activities and medicinal properties for the treatment of cancer, atherosclerosis, diabetes, obesity, and microbial infections.<sup>13,14</sup> CUR provides strong anti-inflammatory effects against the SARS-CoV-2-induced cytokine storm.<sup>15,16</sup> Several pre-clinical and clinical studies have revealed that CUR and its analogues (e.g., diarylpentanoids) significantly attenuate the levels of pro-inflammatory cytokines *viz.*, IL-1, IL-6, IL-8, and TNF- $\alpha$ .<sup>17</sup>

However, the anti-inflammatory effectiveness of CUR is restricted because of its poor bioavailability.<sup>16</sup> Numerous approaches have been used to enhance the bioavailability of CUR including the use of piperine as an adjuvant agent, liposome-based CUR, and phospholipid CUR complexes.<sup>18</sup> Organic nanoparticle (NP)-mediated CUR delivery could be an effective approach to increase its bioavailability, and also sustained and controlled release.<sup>19–21</sup> Organic NPs may enhance the anti-inflammatory potential of CUR and also minimize the quantity of CUR required. The large surface area and small size of NPs provide greater stability and can readily internalize into the cells without compromising its efficacy and integrity. Several recent investigations using cell lines and animal models suggest that inorganic NPs of CUR as a therapeutic agent is more powerful than bulk CUR.<sup>16,18,22</sup> Since organic NPs are nontoxic, biocompatible, biodegradable, and non-immunogenic, the organic NPs of CUR have the

potential to be used as a safe and effective drug against COVID-19.

Therefore, we investigated the anti-inflammatory efficacy of CUR-encapsulated polysaccharide NPs (CUR–PS-NPs) targeting the SARS-CoV-2 spike protein (CoV2-SP)-induced cytokine storm, and compared it with bulk CUR (B-CUR) in liver and lung epithelial cells. We deciphered the mechanism(s) of actions underlying the NF- $\kappa$ B signaling inhibition and MAPK deactivation by CUR that inhibit CoV2-SP-induced cytokine storms. We also investigated the role of CUR in reducing CoV2-SP-mediated phosphorylation of p38 MAPK, p42/44 MAPK, p65/NF- $\kappa$ B, and nuclear p65/NF- $\kappa$ B expression, and release of cytokines, chemokines, and growth factors linked with the liver and lung epithelial cell injury.

## RESULTS AND DISCUSSION

**Preparation and Characterization of CUR–PS-NPs and *In Vitro* Release Kinetics of CUR.** We used an emulsion solvent evaporation process to prepare CUR–PS-NPs (Figure 1a–c).<sup>23</sup> Scanning electron microscopy (SEM) images showed the uniform spherical shape of the CUR–PS-NPs with particle size in the range of 18–27 nm (Figure 1d). The morphology of these NPs was observed using transmission electron microscopy (TEM). The average size of CUR–PS-NPs was  $22 \pm 4$  nm, and the particles distributed uniformly in PS matrix in spherical shapes (Figure 2a). The mean hydrodynamic size and zeta potential of CUR–PS-NPs measured through the dynamic light scattering (DLS) technique revealed that the mean size was  $43 \pm 5$  nm, and the particles exhibited a low (0.52) polydispersity index (PDI), confirming the formation of monodispersed CUR-PS-NPs (Figure 2b). Zeta potential/surface charge of the CUR–PS-NPs was  $-18 \pm 1.6$  mV (Figure 2b). We determined the entrapment efficiency of CUR in a PS matrix, which was  $\sim 25 \pm 2\%$ . In other words, 1 mg of CUR–PS-NPs encapsulated  $250 \mu\text{g}$  of CUR (Figure 2b). All these data confirmed that the size of CUR–PS-NPs was within the nanomaterial range. The observed bigger size in DLS

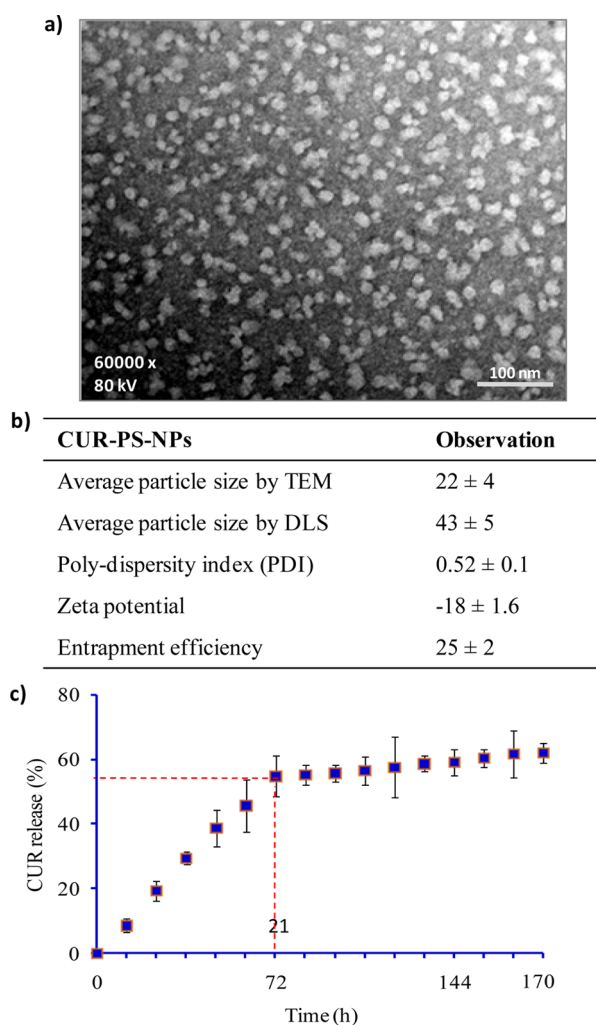


**Figure 2.** Characterization of CUR-PS-NPs. (a) TEM image of CUR-PS-NPs. Scale bar: 100 nm. (b) Measurement of size by TEM and DLS, entrapment efficiency, PDI and zeta-potential of CUR-PS-NPs. (c) Percent release kinetics of CUR from the CUR-PS-NPs. Results are expressed as mean ± SEM of three individual experiments.

analysis than that in TEM was attributed to the hydrodynamic size measurement in the former and the absolute size measurement in the later.<sup>18</sup>

The Fourier-Transform Infrared Spectroscopy (FT-IR) analysis revealed that OH, C-H, and C=O stretching vibrations of PS fraction peaked at  $3429 \pm 4$ ,  $2923 \pm 3$  and  $1637 \pm 3 \text{ cm}^{-1}$ , respectively, which got shifted to  $3531 \pm 5$ ,  $3014 \pm 4$ , and  $1703 \pm 3 \text{ cm}^{-1}$ , respectively, in case of CUR-PS-NPs, indicating that electrostatic interactions took place between CUR and PS of *C. longa* rhizome.<sup>24</sup> CUR-PS-NPs remained stable even after 12 months of preparation at room temperature.

We assessed the release kinetics of CUR from the CUR-PS-NPs for 170 h in a water and ethanol solution (1:1 ratio) at  $37 \pm 1 \text{ }^\circ\text{C}$ . We observed an exponential release up to 72 h achieving 55% of CUR liberation, and in total ~63% of the entrapped CUR was released in 170 h (Figure 2c). These results confirmed the sustained release of CUR from the CUR-PS-NPs.

**CUR-PS-NPs Inhibit Interaction between Human ACE2 and CoV2-SP.** To examine if CUR-PS-NPs attenuate the interaction between human ACE2 and CoV2-SP, we used

an ELISA-based assay in which biotinylated purified human ACE-2 protein binds with the immobilized CoV2-SP.<sup>25</sup> ACE2, a cellular receptor present on the outer surface of a range of human cells and tissues, is the first host cell target of CoV2-SP.<sup>26</sup> Thus, disrupting the interaction between CoV2-SP and ACE2 can be an effective strategy to design potential drugs.<sup>27</sup> We used different doses (0.001, 0.01, 0.1, 0.2, 0.5, and  $5.0 \mu\text{M}$ ) of B-CUR and CUR-PS-NPs for this study. CUR-PS-NPs and B-CUR exhibited a dose-dependent inhibitory effect on the interactions between ACE2 and CoV2-SP, while PSNPs did not show any significant effect. However, CUR-PS-NPs at  $5 \mu\text{M}$  concentration showed a significantly greater inhibitory effect (69.3%) than B-CUR (21.7%) (Figure 3a). This firmly establishes the strong inhibitory effect of CUR-PS-NPs on the interactions between ACE2 and CoV2-SP.

Inhibition of the CoV2-SP and ACE2 interaction by CUR-PS-NPs was further assessed in epithelial cells such as Huh7.5 (liver) and A549 (lung), exposed to 5 nM of CoV2-SP for 24 h following the method given by Gasparello *et al.*<sup>28</sup> We analyzed the expression of ACE2 by RT-PCR. The mRNA expression of ACE2 was significantly decreased in CoV2-SP-exposed lung epithelial cells, while the ACE2 level was enhanced significantly in CUR-PS-NPs-treated Huh7.5 and A549 cells (Figure 3b,c). This confirms that CoV2-SP induces inhibition of ACE2 expression in lung epithelial cells, and CUR-NS-NPs enhance mRNA expression of ACE2.<sup>7</sup> These results further confirm that the CUR-PS-NPs have significantly greater potential to inhibit the interactions between human ACE2 receptor and CoV2-SP than B-CUR and PSNPs.

**Effects of CUR-PS-NPs on Cell Viability and Internalization of CUR.** In order to assess if the cell viability is a factor for the observed inhibitory effect of CUR-PS-NPs on the interaction between human ACE2 and CoV2-SP in epithelial cells, we evaluated the effects of CUR-PS-NPs and B-CUR (0.1, 0.2, 0.5, 5, and  $10 \mu\text{M}$ ) on cell viability by the Alamar blue assay. After 24 h of exposure to CUR-PS-NPs and B-CUR, we found no significant effect on the cell viability of both liver Huh7.5 and lung A549 epithelial cells up to  $5 \mu\text{M}$  concentration. However, at  $10 \mu\text{M}$  dose, the viability of cells got reduced significantly (Figure 4a,b). We further confirmed if  $5 \mu\text{M}$  concentration produces non-lethal effects of CUR-PS-NPs and B-CUR by FACS analysis and fluorescence microscopy using Annexin V-FITC-PI in both Huh7.5 and A549 cells. At  $5 \mu\text{M}$  concentration, CUR-PS-NPs and B-CUR did not reduce cell viability in both the cells (Figure 4c-e; Figure S2a,b). Thus, we selected  $5 \mu\text{M}$  concentrations of CUR-PS-NPs and B-CUR for all subsequent cell-based experiments. We prepared the stock ( $50 \mu\text{M}$ ) of the CUR-PS-NPs and B-CUR in water and ethanol solution (1:1 ratio), and further diluted (1:10 ratio) it for all subsequent experiments.

To test if the delivery of CUR into lung A549 epithelial cells is enhanced using PSNPs, internalization of CUR from CUR-PS-NPs was examined by fluorescence microscopy (FM) as curcumin inherently yields green fluorescence under FM. Greater internalization of CUR was noticed in A549 cells, when exposed to  $5 \mu\text{M}$  of CUR-PS-NPs for 2 h in comparison to B-CUR (Figure S3). This confirms the superior bioavailability of nano-CUR than B-CUR.

**CUR-PS-NPs Inhibit CoV2-SP-Mediated Activation of MAPK/NF- $\kappa$ B Axis.** Patra *et al.* reported that CoV2-SP exposure triggers the activation of MAPK and NF- $\kappa$ B signaling in epithelial cells viz., Huh7.5 and A549 cells.<sup>7</sup> This was

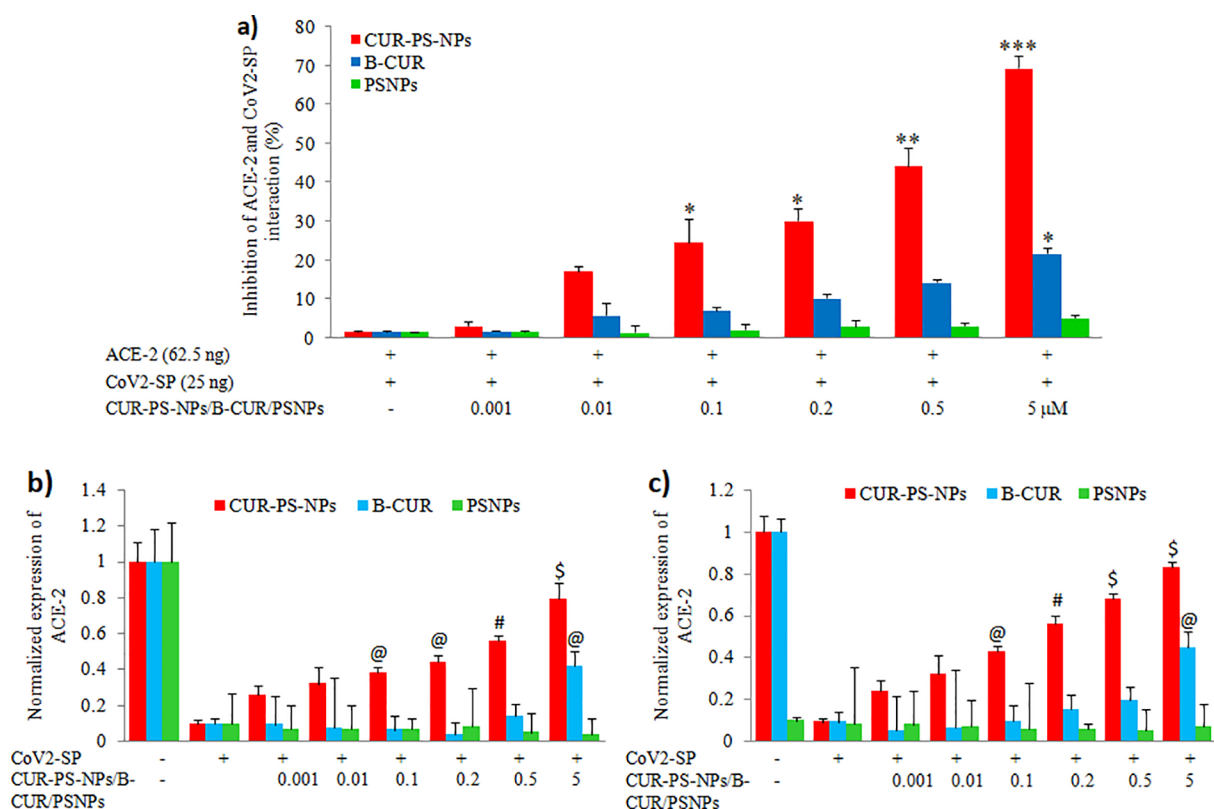


**Figure 3.** Impact of CUR–PS-NPs, B-CUR and PSNPs on human ACE2-CoV2-SP. (a) Concentration dependent effects of CUR–PS-NPs, B-CUR and PSNPs on interaction of ACE2 and CoV2-SP were assessed by ELISA and the results were presented as % inhibition. (b,c) Impact of 24 h treatment of different doses of CUR–PS-NPs and B-CUR on ACE2 mRNA expression in (b) Huh7.5 cells and (c) A549 cells was measured by RT-qPCR analysis. Results are presented as mean  $\pm$  SEM of six individual experiments. “\* $p < 0.05$ ”, “\*\* $p < 0.01$ ” and “\*\*\* $p < 0.001$ ” for unstimulated vs CoV2-SP-stimulated. “@ $p < 0.05$ ”, “# $p < 0.01$ ” and “\$ $p < 0.001$ ” for CoV2-SP-stimulated vs CUR–PS-NPs/B-CUR treated.

concluded based on the higher expression of phosphorylated p38 MAPK (Thr180/Tyr182) and p42/44 MAPK (Thr202/Tyr204) proteins.<sup>7</sup> The elevated MAPK controls p65/NF- $\kappa$ B activation for the production of cytokines.<sup>29</sup> Phosphorylation of NF- $\kappa$ B (Ser276) and I $\kappa$ B $\alpha$  degradation have been reported to trigger transcriptional activation of nuclear p65/NF- $\kappa$ B.<sup>30,31</sup> In our study, we obtained the increased level of phosphorylated NF- $\kappa$ B (Ser276) and reduced I $\kappa$ B $\alpha$  level in Huh7.5 and A549 cells at 5 nM concentration of CoV2-SP (Figure S2). CUR–PS-NPs at the dose of 5  $\mu$ M led to greater reduction in CoV2-SP-induced phospho-p38 MAPK (Thr180/Tyr182), phospho-p42/44 MAPK (Thr202/Tyr204), phosphorylation of p65/NF- $\kappa$ B, and nuclear p65/NF- $\kappa$ B expression in both the epithelial cells compared to B-CUR at similar dose (Figure S4a,b). No significant effect of PSNPs on the levels of these proteins was observed (data not shown). Several investigations have concluded that CoV2-SP is a leading factor in the increased cytokines–inflammatory reaction linked with COVID-19 through activation of MAPK/NF- $\kappa$ B signaling. Some clinical studies with COVID-19 patients have indicated that administration of MAPK/NF- $\kappa$ B blocker medicines results in less chance of hospitalization and admission to the intensive care unit.<sup>32,33</sup> The findings of our study clearly indicate that the CUR–PS-NPs can be used as potential inhibitors of CoV2-SP-induced activation of a MAPK/NF- $\kappa$ B pathway.

**CUR–PS-NPs Block CoV2-SP-Induced IL-6 and IL-8 Production.** IL-6 and IL-8 are two important pro-inflammatory cytokines which are linked to the development of chronic inflammatory diseases.<sup>34</sup> The synthesis of these cytokines is

controlled via MAPK/NF- $\kappa$ B activation that plays a major role in inducing a cytokine storm in COVID-19 patients.<sup>28,35</sup> To establish the role of CUR–PS-NPs in blocking CoV2-SP-induced IL-6 and IL-8 production, we first determined the levels of IL-6 and IL-8 in the culture supernatant of Huh7.5 and A549 cells exposed to 5 nM of CoV2-SP for 24 h by ELISA.<sup>28</sup> An increase in the extracellular IL-6 and IL-8 release was observed in CoV2-SP-stimulated cells compared to unstimulated cells (Figure 5a,b). The stimulated cells were also used to isolate RNA for RT-PCR analysis. The elevated levels of IL-6 and IL-8 were detected in CoV2-SP-stimulated cells which was not the case with unstimulated cells (Figure 5c,d). When CUR–PS-NPs were applied to CoV2-SP-stimulated cells, a significant inhibitory effect on IL-6 and IL-8 levels was detected. Although B-CUR treatment also caused reduction in IL-6 and IL-8 levels it was far less than that of CUR–PS-NPs (Figure 5e–h). This confirms that the inhibition of cytokines production was greater in CUR–PS-NPs-treated Huh7.5 and A549 cells than those treated with B-CUR. The PSNPs treatment alone had no significant inhibitory effects on IL-6 and IL-8 release in CoV2-SP-stimulated Huh7.5 and A549 cells. This suggests that the inhibition of IL-6 and IL-8 levels was due to CUR only, not the PSNPs per se. These data indicate that organic NPs of CUR effectively inhibit cytokine production induced by CoV2-SP in epithelial cells.

**CUR–PS-NPs Regulate CoV2-SP-Induced Expression of Cytokines, Chemokines, and Growth Factors.** Emerging evidences suggest that an excessive production of

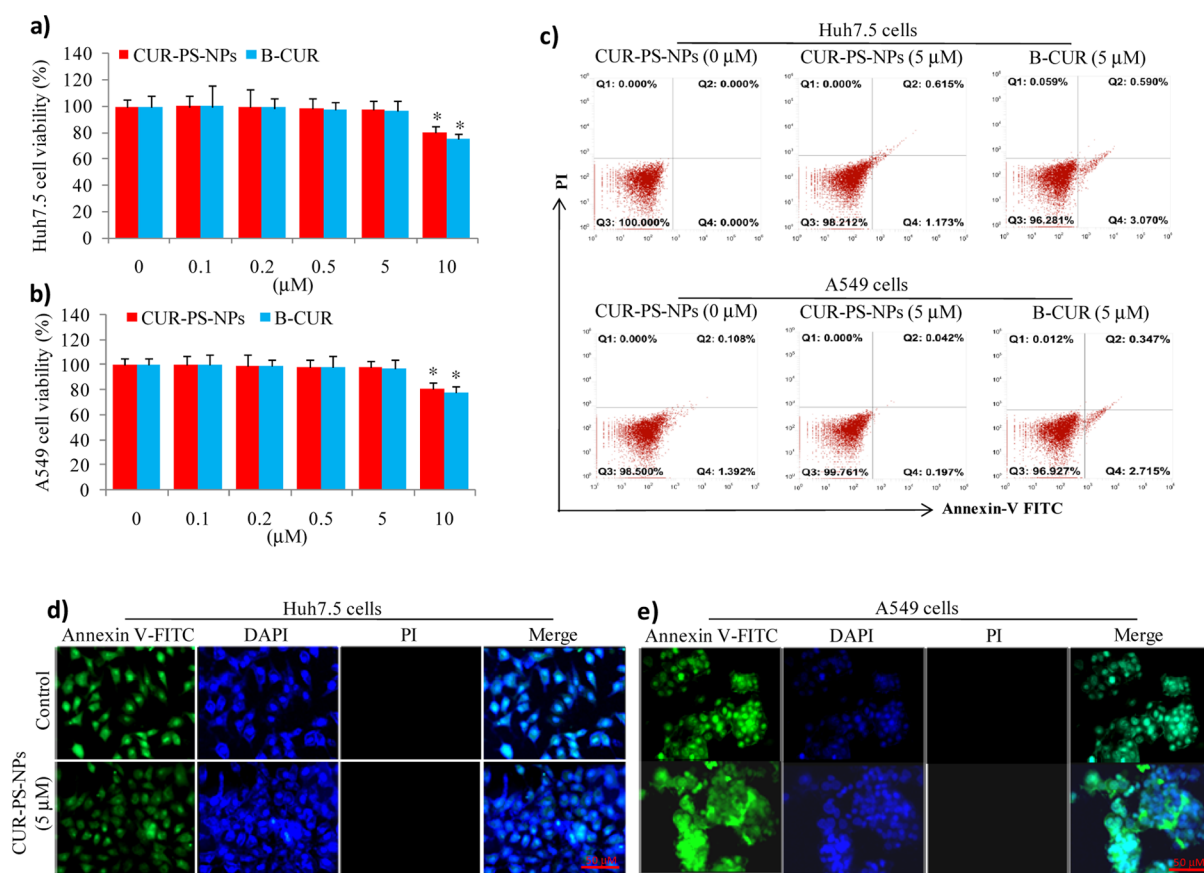


**Figure 4.** Impact of CUR–PS-NPs and B-CUR on cell viability and apoptosis. Cells were exposed to the indicated concentrations of CUR–PS-NPs and B-CUR for 24 h and determined the cell viability using Alamar blue technique in (a) Huh7.5 cells and (b) A549 cells. (c) Detection of cell viability and apoptosis in treated or untreated Huh7.5 cells and A549 cells by flow cytometry using FITC Annexin V and PI staining. Treated or untreated (d) Huh7.5 cells and (e) A549 cells were also analyzed by fluorescence microscope for the detection of cell viability and apoptosis. Results are expressed as mean  $\pm$  SEM of three individual experiments. “\* $p < 0.05$ ” for untreated *vs* CUR–PS-NPs/B-CUR-treated.

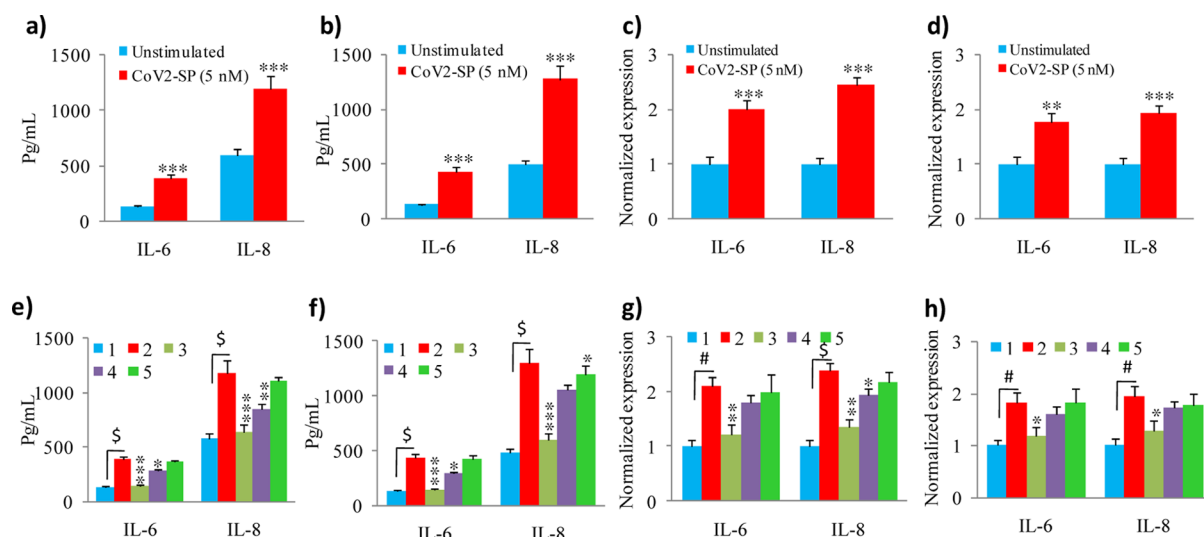


**Figure 5.** Effect of CUR–PS-NPs, B-CUR and PSNPs on CoV2-SP-induced IL-6 and IL-8 mediated storm in epithelial cells. Measurement of IL-6 and IL-8 protein release after 24 h exposure of 5 nM CoV2-SP to (a) Huh7.5 cells and (b) A549 cells. Quantification of IL-6 and IL-8 mRNA expression after 24 h exposure of 5 nM CoV2-SP to (c) liver epithelial Huh7.5 cells and (d) lung A549 epithelial cells. Cells were exposed to 5 nM CoV2-SP for 24 h in the presence or absence of CUR–PS-NPs, B-CUR and PSNPs (5  $\mu$ M). Measurement of IL-6 and IL-8 protein release by ELISA in (e) Huh7.5 cells and (f) A549 cells. Quantification of IL-6 and IL-8 mRNA by RT-qPCR in (g) Huh7.5 cells and (h) A549 cells. Results are presented as mean  $\pm$  SEM of six individual experiments. (1) Unstimulated cells; (2) CoV2-SP-stimulated cells; (3) CoV2-SP-stimulated plus CUR–PS-NPs (5  $\mu$ M); (4) CoV2-SP-stimulated plus B-CUR (5  $\mu$ M); (5) CoV2-SP-stimulated plus PSNPs (5  $\mu$ M). “# $p < 0.05$ ” and “\$ $p < 0.01$ ” for unstimulated *vs* CoV2-SP-stimulated. “\* $p < 0.05$ ”, “\*\* $p < 0.01$ ” and “\*\*\* $p < 0.001$ ” for CoV2-SP-stimulated *vs* CUR–PS-NPs/B-CUR.

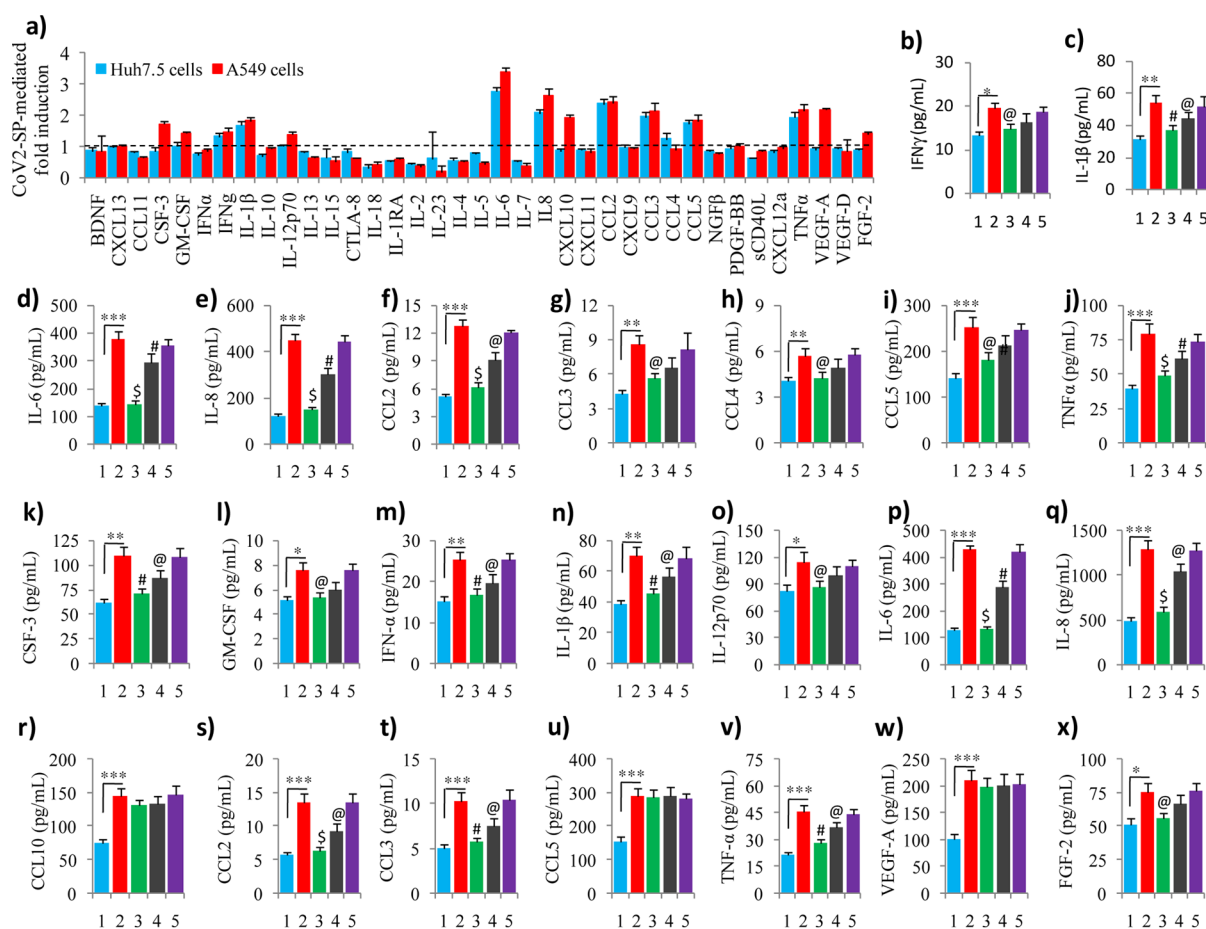


**Figure 6.** Impact of CUR–PS-NPs, B-CUR and PSNPs on the release of cytokines, chemokines and growth factors by CoV2-SP-stimulated epithelial cells. (a) Profile of 37 cytokines, chemokines and growth factors in 24 h stimulation of Huh7.5 cells and A549 cells with 5 nM of CoV2-SP. Released protein levels exceeding the content of 1 pg/mL in the culture medium are presented in the graph. The results are expressed as fold change (CoV2-SP-stimulated cells vs untreated control cells). (b–j). Impacts of CUR–PS-NPs, B-CUR and PSNPs on the inflammation-related cytokines, chemokines and growth factors induced by CoV2-SP in Huh7.5 cells. (k–x) Impacts of CUR–PS-NPs, B-CUR and PSNPs on the inflammation-related cytokines, chemokines and growth induced by CoV2-SP in A549 cells. (1) Untreated and unstimulated cells; (2) CoV2-SP-stimulated cells; (3) CoV2-SP-stimulated plus CUR–PS-NPs (5 μM); (4) CoV2-SP-stimulated plus B-CUR (5 μM); (5) CoV2-SP-stimulated plus PSNPs (5 μM). Results are presented as mean ± SEM of six individual experiments. “\* $p < 0.05$ ”, “\*\* $p < 0.01$ ” and “\*\*\* $p < 0.001$ ” for unstimulated vs CoV2-SP-stimulated. “@ $p < 0.05$ ”, “# $p < 0.01$ ” and “\$ $p < 0.001$ ” for CoV2-SP-stimulated vs CUR–PS-NPs/B-CUR.

circulatory biomarkers of inflammation including cytokines (IL-1, IL-6, and IL-12), chemokines (CXCL8, MCP-1, and IP-10), and growth factors (CCL3 and VEGF) is responsible for the occurrence of ARDS in COVID-19 patients.<sup>36</sup> IP-10 (CXCL10) is also used as a key prognostic marker for SARS disease development.<sup>37</sup> Although the levels of circulatory VEGF remain high in SARS-CoV-2 infected patients, no difference has been observed between severe and mild patients.<sup>38</sup> We used ProcartaPlex analysis to examine the effects of CUR–PS-NPs, B-CUR, and PSNPs (μM) on the expression of inflammatory biomarkers (Table S3). Biomarkers having more than 1 pg/mL concentration in the culture medium of CoV2-SP-induced cells were considered for further assessment. After incubation of 24 h, CoV2-SP-induced Huh7.5 cells showed an elevated secretion of nine proteins viz., IFN $\gamma$ , IL-1 $\beta$ , IL-6, IL-8, CCL2 (MCP-1), CCL3 (MIP-1 $\alpha$ ), CCL4 (MIP-1 $\beta$ ), CCL5 (RANTES), and TNF $\alpha$ , while 14 proteins viz., CSF-3 (G-CSF), GM-CSF, IFN $\gamma$ , IL-1 $\beta$ , IL-12p70, IL-6, IL-8, IP-10 (CXCL10), CCL2, CCL3, CCL5, TNF $\alpha$ , VEGF-A, and FGF-2 got elevated secretion in A549 cells (Figure 6a). In addition to IL-6 and IL-8, we found

greater inhibition in respect of these proteins in CUR–PS-NPs-treated Huh7.5 cells (Figure 6b–j) and A549 cells (Figure 6k–x) as compared to B-CUR and PSNPs-treated cells, with an exception of CCL10, CCL5 and VEGF-A in A549 cells. Treatment of CUR–PS-NPs, B-CUR and PSNPs had no effect on unstimulated Huh7.5 cells (Figure S5a–i) and A549 cells (Figure S6a–n). These results confirm that organic NPs of CUR have a high potential to reduce COVID-19-induced cytokine storm-related inflammation and organ injuries, particularly the lungs and liver.

## CONCLUSIONS

We prepared the organic NPs of CUR using polysaccharide-rich fraction of turmeric rhizome in this study, which inhibited the cytokine storm induced by human CoV2-SP in liver Huh7.5 and lung A549 epithelial cells. Treatment of CoV2-SP-stimulated epithelial cells with CUR–PS-NPs potently inhibited the release of cytokines, chemokines, and growth factors that cause epithelial cell damage through deactivation of NF- $\kappa$ B/MAPK signaling pathway. However, further *in vivo* studies are required to confirm the potential of CUR-PS-NPs

inhibitors of cytokine storm induced by CoV2-SP in liver and lung epithelial cells.

## EXPERIMENTAL PROCEDURES

**Materials.** We bought CUR with more than 97% purity from Sigma-Aldrich, St. Louis, MO, the USA. We obtained purified SARS-CoV-2 spike recombinant glycoprotein and biotinylated recombinant human ACE2 from Abcam (Cambridge, UK). All other analytical grade reagents were used as received without additional purification.

**Isolation and Characterization of PS-Rich Fraction.** We grinded the dried rhizomes of *C. longa* (250 g) which are collected from Shillong, Meghalaya to make a coarse size powder and soaked it in 500 mL of water for 60 min. After refluxing for 120 min, the mixture was centrifuged at 8000 rpm for 30 min. We fractionated the supernatant with ethyl acetate and *n*-butanol. The remaining water layer was mixed properly with ethanol in the ratio of 1:1 and centrifuged to obtain a precipitated material.<sup>39</sup> The yield of fraction was 0.74%. The composition of fraction was also determined by gas chromatography–mass spectrometry (GC–MS) equipped with a TR 50-MS capillary column (30 m × 0.32 mm) and flame ionization detector (Thermo Scientific DSQ II GC–MS system) in a temperature gradient of 100–280 °C at 10 °C/min. The fraction comprised D-glucose (49%), L-rhamnose (14%), D-galacturonic acid (27%), L-arabinose (4%), and D-galactose (6%) (Table S1). The fraction was hydrolyzed at 100 °C for using 2 M of sulphuric acid, followed by acetylation as reported by Huang and colleagues.<sup>40</sup>

**Preparation and Characterization of CUR–PS-NPs.** We used an emulsion solvent evaporation technique to prepare CUR–PS-NPs with minor changes.<sup>23</sup> For this, we dissolved CUR (50 mg) in acetone (1.25 mL) and 250 mg of the fraction in dichloromethane (4 mL) and mixed it together under stirring conditions at 250 rpm for 120 min. We added polyvinyl alcohol solution (1%) to the mixture and stirred for 8 h for removal of organic solvents. Afterward, centrifugation at 9500 rpm for 45 min under 4 °C was carried out. We re-suspended pellets in water and centrifuged, and the process was repeated thrice. Eventually, to achieve a solid dry powder, NPs were freeze-dried using a lyophilizer (Labconco, USA) and stored at 4 °C under anhydrous conditions for until use.

We recorded optical extinction spectra of CUR–PS-NPs by a UV–Vis spectrophotometer (Evolution 201, Thermo, USA) with the help of cuvettes (2 × 2 mm). We determined the hydrodynamic size and zeta potential and PDI of CUR–PS-NPs by performing DLS analysis using a Zetasizer system (MAL1010294 Malvern, UK). We calculated the size and PDI from three individual analyses through intensity distribution. We also examined the morphology and size distribution of CUR–PS-NPs at 80 kV using carbon-coated copper grids by a TEM (JEM-2100, JEOL).

**Assessment of Interaction between Human ACE2 and CoV2-SP.** We assessed the interactions between human ACE2 and CoV2-SP using an ELISA kit (Biosystems, USA), according to the manufacturer's instructions. Briefly, we coated each well of the microtiter plate (Genaxy Scientific, India) with CoV2-SP (25 ng) for 12 h, followed by careful three washings with phosphate-buffered saline (PBS) (pH 7.2). We added different concentrations of CUR–PS-NPs and B-CUR (5–25 µg/mL) to each well, followed by addition of biotinylated recombinant human ACE2 (62.5 ng), incubated at 37 °C for 30 min, and maintained a total volume of 100 µL in each well. The sample without inhibitor was considered as a negative control. For the detection of interactions between CoV2-SP and ACE2, we added streptavidin-HRP (horse-radish peroxidase) and peroxidase substrate (3,3',5,5'-tetramethylbenzidine). We recorded the absorbance at 450 nm using a Synergy/HTX microplate reader (BioTek, Germany).

**Cell Culture.** We procured lung epithelial A549 cells and liver epithelial Huh7.5 cells from American Type Culture Collection (ATCC)-recognized cell repository at National Centre for Cell Sciences, Pune, India. We cultured cells in a humidified atmosphere at 37 °C with 5% CO<sub>2</sub> in Dulbecco's modified Eagle's medium (DMEM) (Gibco, Thermo Fisher Scientific) supplemented with

heat-inactivated fetal bovine serum (10%) (MP Biomedicals), penicillin (100 U/mL), and streptomycin (100 mg/mL) (MP Biomedicals).

**Analysis of Cell Viability.** We evaluated cell viability by the Alamar blue assay, and FACS analysis and fluorescence microscopy using Annexin V-FITC and PI that measured cell apoptosis in treated or untreated epithelial cells.<sup>41</sup> After treatment of 24 h, 25 µL of the Alamar blue dye (Thermo Fisher Scientific) was added to each well, and cells were incubated for 2 h in CO<sub>2</sub> incubator at 37 °C. We measured the absorbance at 570 and 600 nm using a Synergy/HTX microplate reader (BioTek, Germany). For FACS analysis, trypsinized cells were washed twice with 1× PBS. After addition of 100 µL binding buffer (BF) containing 5 µL of Annexin V-FITC and PI, we incubated cells in the dark for 15 min. We added 400 µL of BF to the cells and analyzed using Attune NxT flow cytometry with Attune NxT version 2.6 software (Thermo Fisher Scientific) and fluorescence microscope (Leica DCF 700 T, Germany).

**Stimulation of Epithelial Cells with CoV2-SP.** We prepared a stock solution of 7.2 µM CoV2-SP in urea (9%), Tris-HCl (0.32%; pH 7.2) and 50% glycerol, and diluted in DMEM medium (200 µL) to attain the final doses applied to treat epithelial cells as recently reported by Gasparello *et al.*<sup>28</sup> We seeded cells (5 × 10<sup>5</sup> cells/mL) and incubated until 50% of confluence. Afterward, cells were exposed with CoV2-SP (5 nM). To achieve maximum spike protein interaction with the receptor, we incubated these cells for 30 min at 4 °C as reported by Wang and colleagues.<sup>42</sup> Then, the final volume of 500 µL was made up by adding DMEM medium. We further incubated cells at 37 °C for 24 h. We treated cells with DMSO (Sigma-Aldrich, USA) for the consideration as unstimulated cells and used these cells as reference controls.

**RNA Extraction and RT-qPCR Reactions.** Trypsinized cells were washed thrice with 1× PBS. We isolated total RNA from obtained cell pallets using an RNeasy mini kit (Qiagen, USA) according to the manufacturer's protocol. We washed the isolated RNA with cold ethanol (75%) once, and after drying RNA pallets were re-dissolved in nuclease-free water.

We prepared cDNA using a Verso complementary DNA (cDNA) synthesis kit (Applied Biosystem, Thermo Fischer Scientific) according to manufacturer's instructions. We amplified 2 µL of cDNA in the presence of a SYBR green PCR master mix (Thermo Fisher, USA) and 800 nM primer for 40 cycles according to manufacturer's instructions using a real-time PCR system (7900HT; Applied Biosystems, USA). We calculated relative expression of each gene using the comparative cycle threshold  $\Delta\Delta C_t$  method. We used  $\beta$ -actin as an internal reference control to normalize the gene expression. No template cDNA as a negative control was also used in each experiment to study specificity and to exclude contamination. We carried out RT-qPCR experiments in triplicate for both target and normalize genes. The gene-specific primers were designed using Primer 3 version 0.4.0 and used for the amplification of target genes (Table S2).

**Statistical Analysis.** The results are presented as mean ± standard error of the mean (SEM). GraphPad Prism 8 was used to analyze the data. Comparison among treatments was evaluated using analysis of variances (ANOVA). Differences were defined with \*/<sup>@</sup>*p* < 0.05, \*\*/<sup>#</sup>*p* < 0.01 and \*\*\*/<sup>§</sup>*p* < 0.001.

## ASSOCIATED CONTENT

### Supporting Information

The Supporting Information is available free of charge at <https://pubs.acs.org/doi/10.1021/acsabm.1c00874>.

FT-IR spectra of PS fraction and CUR–PS-NPs, impact of B-CUR on cell viability and apoptosis, internalization of CUR–PS-NPs and B-CUR inside the lung A549 epithelial cells, impact of CUR–PS-NPs and B-CUR on MAPK/NF- $\kappa$ B signaling in epithelial cells, effect of CUR–PS-NPs and B-CUR on the release of cytokines, chemokines and growth factors in liver epithelial Huh7.5

cells, effect of CUR–PS-NPs and B-CUR on the release of cytokines, chemokines and growth factors in lung epithelial A549 cells, PS composition of isolated fraction, list of primers, and list of used cytokines/chemokines/growth factors and methodologies of immunoblot and profiling of cytokines/chemokines/growth factors (PDF)

## AUTHOR INFORMATION

### Corresponding Authors

**Brahma N. Singh** – Pharmacology Division, CSIR-National Botanical Research Institute, Lucknow 226001, India;

orcid.org/0000-0002-9296-1380;

Email: singhbrahmanand99@gmail.com

**Saroj K. Barik** – Pharmacology Division, CSIR-National Botanical Research Institute, Lucknow 226001, India;

Email: sarojkbarik@gmail.com

### Authors

**Vivek K. Sharma** – Pharmacology Division, CSIR-National Botanical Research Institute, Lucknow 226001, India

**Prateeksha** – Pharmacology Division, CSIR-National Botanical Research Institute, Lucknow 226001, India

**Shailendra P. Singh** – Department of Botany, Banaras Hindu University, Varanasi 221005, India

**Chandana V. Rao** – Pharmacology Division, CSIR-National Botanical Research Institute, Lucknow 226001, India

Complete contact information is available at:

<https://pubs.acs.org/10.1021/acsabm.1c00874>

### Author Contributions

<sup>§</sup>Vivek K. Sharma and Prateeksha contributed equally. Vivek K. Sharma: Performed experiments, data analysis. Prateeksha: Performed experiments, Ddata analysis. Sailendra P. Singh: Writing. Brahma N. Singh. Conceptualization, funding, friting – feview and editing. Chandana V. Rao: Data analysis. Saroj K. Barik: Conceptualization, funding, writing review and editing.

### Notes

The authors declare no competing financial interest.

## ACKNOWLEDGMENTS

This work was supported by Council of Scientific and Industrial Research (CSIR), New Delhi, India under in-house project OLP-0106 and Department of Biotechnology (DBT), New Delhi, India project No. BT/01/17/ 835 NE/TAX.

## REFERENCES

- (1) Prateeksha, G.; Rana, T. S.; Asthana, A. K.; Singh, B. N.; Barik, S. K. Screening of cryptogamic secondary metabolites as putative inhibitors of SARS-CoV-2 main protease and ribosomal binding domain of spike glycoprotein by molecular docking and molecular dynamics approaches. *J. Mol. Struct.* **2021**, *1240*, 130506.
- (2) Wang, X.; Xu, W.; Hu, G.; Xia, S.; Sun, Z.; Liu, Z.; Xie, Y.; Zhang, R.; Jiang, S.; Lu, L. SARS-CoV-2 infects T lymphocytes through its spike protein-mediated membrane fusion. *Cell. Mol. Immunol.* **2020**, *17*, 894.
- (3) Zhu, N.; Zhang, D.; Wang, W.; Li, X.; Yang, B.; Song, J.; Zhao, X.; Huang, B.; Shi, W.; Lu, R.; Niu, P.; Zhan, F.; Ma, X.; Wang, D.; Xu, W.; Wu, G.; Gao, G. F.; Tan, W.; Coronavirus, C. N. A novel coronavirus from patients with pneumonia in China, 2019. *N. Engl. J. Med.* **2020**, *382*, 727–733.

- (4) Pelaia, C.; Tinello, C.; Vatrella, A.; De Sarro, G.; Pelaia, G. Lung under attack by COVID-19-induced cytokine storm: pathogenic mechanisms and therapeutic implications. *Ther. Adv. Respir. Dis.* **2020**, *14*, 1753466620933508.

- (5) Wrapp, D.; Wang, N.; Corbett, K. S.; Goldsmith, J. A.; Hsieh, C.-L.; Abiona, O.; Graham, B. S.; McLellan, J. S. Cryo-EM structure of the 2019-nCoV spike in the prefusion conformation. *Science* **2020**, *367*, 1260–1263.

- (6) Ratajczak, M. Z.; Bujko, K.; Ciechanowicz, A.; Sielatycka, K.; Cymer, M.; Marlicz, W.; Kucia, M. SARS-CoV-2 entry receptor ACE2 is expressed on very small CD45(-)precursors of hematopoietic and endothelial cells and in response to virus spike protein activates the Nlrp3 inflammasome. *Stem Cell Rev. Rep.* **2021**, *17*, 266–277.

- (7) Patra, T.; Meyer, K.; Geerling, L.; Isbell, T. S.; Hoft, D. F.; Brien, J.; Pinto, A. K.; Ray, R. B.; Ray, R. SARS-CoV-2 spike protein promotes IL-6 trans-signaling by activation of angiotensin II receptor signaling in epithelial cells. *PLoS Pathog.* **2020**, *16*, No. e1009128.

- (8) Matthay, M. A.; Leligdowicz, A.; Liu, K. D. Biological Mechanisms of COVID-19 Acute Respiratory Distress Syndrome. *Am. J. Respir. Crit. Care Med.* **2020**, *202*, 1489–1491.

- (9) Soumagne, T.; Winiszewski, H.; Besch, G.; Mahr, N.; Senot, T.; Costa, P.; Grillet, F.; Behr, J.; Mouhat, B.; Mourey, G.; Fournel, A.; Meneveau, N.; Samain, E.; Capellier, G.; Piton, G.; Pili-Floury, S. Pulmonary embolism among critically ill patients with ARDS due to COVID-19. *Respir. Med.* **2020**, *78*, 100789.

- (10) Grasselli, G.; Tonetti, T.; Protti, A.; Langer, T.; Girardis, M.; Bellani, G.; Laffey, J.; Carrafiello, G.; Carsana, L.; Rizzuto, C.; Zanella, A.; Scaravilli, V.; Pizzilli, G.; Grieco, D. L.; Di Meglio, L.; de Pascale, G.; Lanza, E.; Monteduro, F.; Zompatori, M.; Filippini, C.; Locatelli, F.; Cecconi, M.; Fumagalli, R.; Nava, S.; Vincent, J.-L.; Antonelli, M.; Slutsky, A. S.; Pesenti, A.; Ranieri, V. M.; Lissoni, A.; Rossi, N.; Guzzardella, A.; Valsecchi, C.; Madotto, F.; Bevilacqua, F.; Di Laudo, M.; Querci, L.; Seccafico, C. Pathophysiology of COVID-19-associated acute respiratory distress syndrome: a multicentre prospective observational study. *Lancet Respir. Med.* **2020**, *8*, 1201–1208.

- (11) Nasonov, E.; Samsonov, M. The role of Interleukin 6 inhibitors in therapy of severe COVID-19. *Biomed. Pharmacother.* **2020**, *131*, 110698.

- (12) Andreakos, E.; Papadaki, M.; Serhan, C. N. Dexamethasone, pro-resolving lipid mediators and resolution of inflammation in COVID-19. *Allergy* **2021**, *76*, 626–628.

- (13) Aggarwal, B. B.; Shishodia, S. Molecular targets of dietary agents for prevention and therapy of cancer. *Biochem. Pharmacol.* **2006**, *71*, 1397–1421.

- (14) Jadaun, V.; Prateeksha, P.; Singh, B. R.; Paliya, B. S.; Upreti, D. K.; Rao, C. V.; Rawat, A. K. S.; Singh, B. N. Honey enhances the anti-quorum sensing activity and anti-biofilm potential of curcumin. *RSC Adv.* **2015**, *5*, 71060–71070.

- (15) Liu, Z.; Ying, Y. The inhibitory effect of curcumin on virus-induced cytokine storm and its potential use in the associated severe pneumonia. *Front. Cell Dev. Biol.* **2020**, *8*, 479.

- (16) Prateeksha; Rao, C. V.; Das, A. K.; Barik, S. K.; Singh, B. N. ZnO/curcumin nanocomposites for enhanced inhibition of *Pseudomonas aeruginosa* Virulence via LasR-RhlR quorum sensing systems. *Mol. Pharm.* **2019**, *16*, 3399–3413.

- (17) Zhang, B.; Swamy, S.; Balijepalli, S.; Panicker, S.; Mooliyil, J.; Sherman, M. A.; Parkkinen, J.; Raghavendran, K.; Suresh, M. V. Direct pulmonary delivery of solubilized curcumin reduces severity of lethal pneumonia. *Faseb. J.* **2019**, *33*, 13294–13309.

- (18) Tiwari, S. K.; Agarwal, S.; Seth, B.; Yadav, A.; Nair, S.; Bhatnagar, P.; Karmakar, M.; Kumari, M.; Chauhan, L. K. S.; Patel, D. K.; Srivastava, V.; Singh, D.; Gupta, S. K.; Tripathi, A.; Chaturvedi, R. K.; Gupta, K. C. Curcumin-loaded nanoparticles potently induce adult neurogenesis and reverse cognitive deficits in Alzheimer's disease model via canonical Wnt/beta-catenin pathway. *ACS Nano* **2019**, *13*, 7355.

- (19) Singh, B. N.; Prateeksha; Gupta, V. K.; Chen, J.; Atanasov, A. G. Organic nanoparticle-based combinatory approaches for gene therapy. *Trends Biotechnol.* **2017**, *35*, 1121–1124.
- (20) Prateeksha, P.; Bajpai, R.; Rao, C. V.; Upreti, D. K.; Barik, S. K.; Singh, B. N. Chrysofanol-functionalized silver nanoparticles for anti-adhesive and anti-biofouling coatings to prevent urinary catheter-associated infections. *ACS Appl. Nano Mater.* **2021**, *4*, 1512–1528.
- (21) Singh, B. N.; Singh, B. R.; Gupta, V. K.; Kharwar, R. N.; Pecoraro, L. Coating with microbial hydrophobins: a novel approach to develop smart drug nanoparticles. *Trends Biotechnol.* **2018**, *36*, 1103–1106.
- (22) Karthikeyan, A.; Senthil, N.; Min, T.; Nanocurcumin. A promising candidate for therapeutic applications. *Front. Pharmacol.* **2020**, *11*, 487.
- (23) Tsai, Y.-M.; Chien, C.-F.; Lin, L.-C.; Tsai, T.-H. Curcumin and its nano-formulation: The kinetics of tissue distribution and blood-brain barrier penetration. *Int. J. Pharm.* **2011**, *416*, 331–338.
- (24) Chen, N. D.; Chen, N. F.; Li, J.; Cao, C. Y.; Wang, J. M.; Huang, H. P. Similarity evaluation of different origins and species of dendrobiums by GC-MS and FTIR analysis of polysaccharides. *Int. J. Anal. Chem.* **2015**, *2015*, 713410.
- (25) Balkrishna, A.; Haldar, S.; Singh, H.; Roy, P.; Varshney, A. Coronil, a tri-herbal formulation, attenuates spike-protein-mediated sars-cov-2 viral entry into human alveolar epithelial cells and pro-inflammatory cytokines production by inhibiting spike protein-ACE-2 interaction. *J. Inflamm. Res.* **2021**, *14*, 869–884.
- (26) Wan, Y.; Shang, J.; Graham, R.; Baric, R. S.; Li, F. Receptor Recognition by the Novel Coronavirus from Wuhan: an Analysis Based on Decade-Long Structural Studies of SARS Coronavirus. *J. Virol.* **2020**, *94*, No. e00127.
- (27) Ali, A.; Vijayan, R. Dynamics of the ACE2–SARS-CoV-2/SARS-CoV spike protein interface reveal unique mechanisms. *Sci. Rep.* **2020**, *10*, 14214.
- (28) Gasparello, J.; D'Aversa, E.; Papi, C.; Gambari, L.; Grigolo, B.; Borgatti, M.; Finotti, A.; Gambari, R. Sulforaphane inhibits the expression of interleukin-6 and interleukin-8 induced in bronchial epithelial IB3-1 cells by exposure to the SARS-CoV-2 Spike protein. *Phytomedicine* **2021**, *87*, 153583.
- (29) Kumar, S.; Boehm, J.; Lee, J. C. p38 map kinases: Key signalling molecules as therapeutic targets for inflammatory diseases. *Nat. Rev. Drug Discovery* **2003**, *2*, 717–726.
- (30) Singh, B. N.; Singh, H. B.; Singh, A.; Naqvi, A. H.; Singh, B. R. Dietary phytochemicals alter epigenetic events and signaling pathways for inhibition of metastasis cascade: Phytoblockers of metastasis cascade. *Cancer Met. Rev.* **2014**, *33*, 41–85.
- (31) Singh, B. N.; Shankar, S.; Srivastava, R. K. Green tea catechin, epigallocatechin-3-gallate (EGCG): Mechanisms, perspectives and clinical applications. *Biochem. Pharmacol.* **2011**, *82*, 1807–1821.
- (32) Hariharan, A.; Hakeem, A. R.; Radhakrishnan, S.; Reddy, M. S.; Rela, M. The role and therapeutic potential of nf-kappa-b pathway in severe COVID-19 patients. *Inflammopharmacology* **2021**, *29*, 91–100.
- (33) Zarrin, A. A.; Bao, K.; Lupardus, P.; Vucic, D. Kinase inhibition in autoimmunity and inflammation. *Nat. Rev. Drug Discovery* **2021**, *20*, 39–63.
- (34) Singh, B. N.; Prateeksha, A. K.; Rawat, A. K. S.; Bhagat, R. M.; Singh, B. R. Black tea: Phytochemicals, cancer chemoprevention, and clinical studies. *Crit. Rev. Food Sci. Nutr.* **2017**, *57*, 1394–1410.
- (35) Brasier, A. R. The nuclear factor-kappaB-interleukin-6 signalling pathway mediating vascular inflammation. *Cardiovasc. Res.* **2010**, *86*, 211–218.
- (36) Coperchini, F.; Chiovato, L.; Croce, L.; Magri, F.; Rotondi, M. The cytokine storm in COVID-19: An overview of the involvement of the chemokine/chemokine-receptor system. *Cytokine Growth Factor Rev.* **2020**, *53*, 25–32.
- (37) Jiang, Y.; Xu, J.; Zhou, C.; Wu, Z.; Zhong, S.; Liu, J.; Luo, W.; Chen, T.; Qin, Q.; Deng, P. Characterization of cytokine/chemokine profiles of severe acute respiratory syndrome. *Am. J. Respir. Crit. Care Med.* **2005**, *171*, 850–857.
- (38) Huang, C.; Wang, Y.; Li, X.; Ren, L.; Zhao, J.; Hu, Y.; Zhang, L.; Fan, G.; Xu, J.; Gu, X.; Cheng, Z.; Yu, T.; Xia, J.; Wei, Y.; Wu, W.; Xie, X.; Yin, W.; Li, H.; Liu, M.; Xiao, Y.; Gao, H.; Guo, L.; Xie, J.; Wang, G.; Jiang, R.; Gao, Z.; Jin, Q.; Wang, J.; Cao, B. Clinical features of patients infected with 2019 novel coronavirus in Wuhan, China. *Lancet* **2020**, *395*, 497–506.
- (39) Yue, G. G. L.; Chan, B. C. L.; Hon, P.-M.; Kennelly, E. J.; Yeung, S. K.; Cassileth, B. R.; Fung, K.-P.; Leung, P.-C.; Lau, C. B. S. Immunostimulatory activities of polysaccharide extract isolated from *Curcuma longa*. *Int. J. Biol. Macromol.* **2010**, *47*, 342–347.
- (40) Huang, X. L.; Wu, H. Q.; Huang, F.; Lin, X. S. Analysis of polysaccharide from broken cellular wall and unbroken spore of *Ganoderma lucidum*. *Chin. Tradit. Herb. Drugs* **2006**, *37*, 813–816.
- (41) Singh, B. R.; Singh, B. N.; Khan, W.; Singh, H. B.; Naqvi, A. H. ROS-mediated apoptotic cell death in prostate cancer LNCaP cells induced by biosurfactant stabilized CdS quantum dots. *Biomaterials* **2012**, *33*, 5753–5767.
- (42) Wang, W.; Ye, L.; Ye, L.; Li, B.; Gao, B.; Zeng, Y.; Kong, L.; Fang, X.; Zheng, H.; Wu, Z.; She, Y. Up-regulation of IL-6 and TNF-alpha induced by SARS-coronavirus spike protein in murine macrophages via NF-kappaB pathway. *Virus Res.* **2007**, *128*, 1–8.